An ancient clade of *Penelope*-like retroelements with permuted domains is present in the green lineage and protists, and dominates many invertebrate genomes

Rory J. Craig[1†*], Irina A. Yushenova[2†], Fernando Rodriguez[2], Irina R. Arkhipova[2*]

[1]Institute of Evolutionary Biology, University of Edinburgh, Edinburgh, UK

[2]Josephine Bay Paul Center for Comparative Molecular Biology and Evolution, Marine Biological Laboratory, Woods Hole, MA, USA

*Corresponding author. Email: iarkhipova@mbl.edu; rory.craig@ed.ac.uk.

[†]These authors contributed equally to this work

Running title: Diversity of *Penelope*-like retrotransposons

Key words: transposable elements; retrotransposons; reverse transcriptase; GIY-YIG endonuclease; selenoproteins; microsatellites

ORCID:

0000-0002-6262-0008 (R.C.)

0000-0001-6291-6215 (I.Y.)

0000-0003-4044-8734 (F.R.)

0000-0002-4805-1339 (I.A.)

ABSTRACT

Penelope-like elements (PLEs) are an enigmatic clade of retroelements whose reverse transcriptases (RTs) share a most recent common ancestor with telomerase RTs. The single ORF of canonical EN+ PLEs encodes RT and a C-terminal GIY-YIG endonuclease (EN) that enables intrachromosomal integration, while EN– PLEs lack endonuclease and are generally restricted to chromosome termini. EN+ PLEs have only been found in animals, except for one case of horizontal transfer to conifers, while EN– PLEs occur in several kingdoms. Here we report a new, deep-branching PLE clade with a permuted domain order, whereby an N-terminal GIY-YIG endonuclease is linked to a C-terminal RT by a short domain with a characteristic Zn-finger-like motif. These N-terminal EN+ PLEs share a structural organization, including pseudo-LTRs and complex tandem/inverted insertions, with canonical EN+ PLEs from *Penelope*/*Poseidon*, *Neptune* and *Nematis* clades, and show insertion bias for microsatellites, but lack hammerhead ribozyme motifs. However, their phylogenetic distribution is much broader. The *Naiad* clade is found in numerous invertebrate phyla, where they can reach tens of thousands of copies per genome. *Naiads* in spiders and clams independently evolved to encode selenoproteins. *Chlamys*, which lack the CCHH motif universal to PLE endonucleases, occur in green algae, spike mosses (targeting ribosomal DNA) and the slime mold *Physarum*. Unlike canonical PLEs, RTs of N-terminal EN+ PLEs contain the insertion-in-fingers domain, strengthening the link between PLEs and telomerases. Additionally, we describe *Hydra*, a novel metazoan C-terminal EN+ clade. Overall, we conclude that PLE diversity, distribution and abundance is comparable to non-LTR and LTR-retrotransposons.

INTRODUCTION

Transposable elements (TEs) are characterized by their intrinsic ability to move within and between genomes. In eukaryotes, TEs contribute not only to structural organization of chromosomes and variation in genome size, but also to genetic and epigenetic regulation of numerous cellular processes (Wells and Feschotte 2020). TEs are traditionally divided into two classes, based on the presence (class I, retrotransposons) or absence (class II, DNA transposons) of an RNA intermediate in the transposition cycle. Retrotransposons, in turn, are divided into subclasses based on the presence or absence of long terminal repeats (LTRs): LTR-retrotransposons are framed by direct repeats, phylogenetically close DIRS elements by split inverted repeats, non-LTR retrotransposons lack terminal repeats, and *Penelope*-like elements (PLEs) have a special kind of repeats called pseudo-LTRs (pLTRs), which may be in direct or inverted orientation. Repeat formation in each subclass is associated with the combined action of phylogenetically distinct clades of reverse transcriptase (RT) domain fused to different types of endonuclease/phosphotransferase (EN) domains: DDE-type integrases (IN) or tyrosine recombinases (YR) in LTR-retrotransposons; restriction enzyme-like (REL) or apurinic /apyrimidinic (AP) endonucleases in non-LTR retrotransposons; and GIY-YIG endonucleases in PLEs (Arkhipova 2017). The fusion of EN to RT is typically C-terminal, with the exception of an N-terminal EN in *copia*-like LTR-retrotransposons and in AP-containing non-LTR retrotransposons. The concerted action of RT and EN that combines cleavage and joining of DNA strands with cDNA synthesis during retrotransposition results in characteristic terminal structures that define the boundaries of new insertions.

The GIY-YIG EN domain typically associated with PLEs may have its evolutionary origins in bacterial group I introns, which are not retroelements (Stoddard 2014). The group I intron-encoded homing ENs are characterized by long recognition sequences, and act essentially as monomeric nickases, cleaving DNA on one strand at a time. The relatively short GIY-YIG cleavage module (~70 aa) is often tethered to additional DNA-binding domains for target recognition (Derbyshire, et al. 1997; Van Roey, et al. 2002).

62 In eukaryotic PLEs, the activity of the recombinant GIY-YIG EN has been studied *in*
63 *vitro* for *Penelope* elements of *Drosophila virilis*, where it displayed several properties
64 expected from homology to prokaryotic enzymes, such as functional catalytic residues,
65 nicking activity producing a free 3'-OH for RT priming, and moderate target preferences
66 (Pyatkov, et al. 2004). Variable distance between first-strand cleavage of DNA during
67 target-primed reverse transcription (TPRT) and second-strand cleavage upon TPRT
68 completion dictates the variable length of the target-site duplication (TSD), which is
69 observed at the integration site. Phylogenetically, PLE ENs form a distinct cluster within
70 a large GIY-YIG nuclease superfamily, where diverse homing ENs occupy a central
71 position (Dunin-Horkawicz, et al. 2006). PLE ENs are distinguished from those of
72 homing ENs by the presence of a highly conserved CCHH Zn-finger motif, where the
73 two cysteines are located directly between the GIY and YIG motifs (Arkhipova 2006).
74
75 Phylogenetic history of the longer RT domain is much more informative and reveals a
76 sister relationship between PLEs and telomerase RTs (TERTs), which add G-rich
77 telomeric repeats to extend eukaryotic chromosome ends (Arkhipova, et al. 2003). All
78 described PLEs form two major groups: endonuclease-deficient (EN–) PLEs,
79 retroelements found in several eukaryotic kingdoms at or near telomeres, and
80 endonuclease-containing (EN+) PLEs, which harbor a C-terminal GIY-YIG EN enabling
81 retrotransposition throughout the genome (Fig. 1) (Gladyshev and Arkhipova 2007).
82 Three large EN+ PLE clades have been named *Penelope*/*Poseidon*, *Neptune* and
83 *Nematis*, the latter two being characterized by the presence of an additional conserved
84 Zn-finger motif in the linker between RT and EN (Arkhipova 2006). Two EN– RT clades,
85 *Athena* and *Coprina*, lack the EN domain entirely, but display a unique ability to attach
86 to exposed G-rich telomeric repeat overhangs, assisted by stretches of reverse-
87 complement telomeric repeats combined with adjacent hammerhead ribozyme motifs
88 (HHR) (Gladyshev and Arkhipova 2007; Arkhipova, et al. 2017). Despite the ancient
89 origin of PLEs predating their divergence from TERTs, which are pan-eukaryotic, the
90 phylogenetic distribution of EN+ PLEs has so far been restricted to animals, with one
91 exception of documented horizontal transfer to conifers (Lin, et al. 2016). Here we
92 report the discovery of a novel deep-branching EN+ PLE clade, where the GIY-YIG EN

is unexpectedly positioned N-terminally to the RT. A clade of these elements present in animals, termed *Naiad*, contains the GIY-YIG domain bearing the characteristic Zn-fingers found in canonical EN+ PLEs, while a second group, termed *Chlamys*, are present in green algae, spike mosses and the slime mold *Physarum*, and lack both EN Zn-finger motifs. These results uncover hitherto unknown PLE diversity, which spans all eukaryotic kingdoms, testifying to their ancient origins. We also report that *Naiads* from species as diverse as spiders and clams can code for selenoproteins, which have not previously been described in any TEs.

RESULTS

Novel PLEs with N-terminal location of the GIY-YIG endonuclease domain

While cataloguing PLEs in several recently sequenced genomes, such as the acanthocephalan (*Pomphorhynchus laevis*) and a bdelloid rotifer (*Didymodactylos carnosus*), as well as a darwinulid ostracod (*Darwinula stevensoni*) (Mauer, et al. 2020; Nowell, et al. 2021; Schön, et al. 2021), we noticed the absence of the GIY-YIG domain at the C-terminus of several PLEs, which is typically indicative of EN– PLEs. In these cases, however, extending the 5'-end of the frequently truncated PLE copies revealed a conserved N-terminal GIY-YIG EN domain, typically 220-275 aa in length. A high degree of 5'-truncation apparently precluded earlier identification of this novel type of PLEs. For instance, Repbase, a comprehensive database of eukaryotic TEs (Bao, et al. 2015), contains two PLEs consistently appearing as top RT matches to the novel PLEs, yet having no N-terminal EN domain (*Penelope-2_CGi* from the Pacific oyster *Crassostrea gigas* and *Penelope-1_EuTe* from the Texas clam shrimp *Eulimnadia texana*). We extended the 767-aa *Penelope-2_CGi_1p* consensus in the 5'-direction and compared it with two sibling species, *Crassostrea virginica* and especially *Saccostrea glomerata*, where this element is mostly intact, revealing an N-terminal GIY-YIG domain which brings the total ORF length up to 876 aa in *C. gigas* (still 5'-truncated) and to 1024 aa in *S. glomerata*.

123 We then conducted an extensive database search for representatives of this previously
124 undescribed type of PLEs in sequenced genomes, relying primarily on the N-terminal
125 position of the GIY-YIG domain and several characteristic motifs (see below) to
126 discriminate between novel and canonical PLEs (Fig. 1). Our search revealed a
127 surprising diversity of hosts from eight animal phyla, including ctenophores, cnidarians,
128 rotifers, nematodes, arthropods, mollusks, hemichordates, and vertebrates (fish).
129 Additionally, about a dozen hits on short contigs were annotated as bacterial, however
130 upon closer inspection these were discarded as eukaryotic contaminants from
131 metagenomic assemblies with an incorrect taxonomic assignment (Arkhipova 2020).
132 Out of 36 animal host species, most were aquatic (26), 6 were parasitic, and only 4
133 were free-living terrestrial species (2 spiders and 2 nematodes). We therefore chose the
134 name *Naiad* for this newly discovered type of PLEs.
135

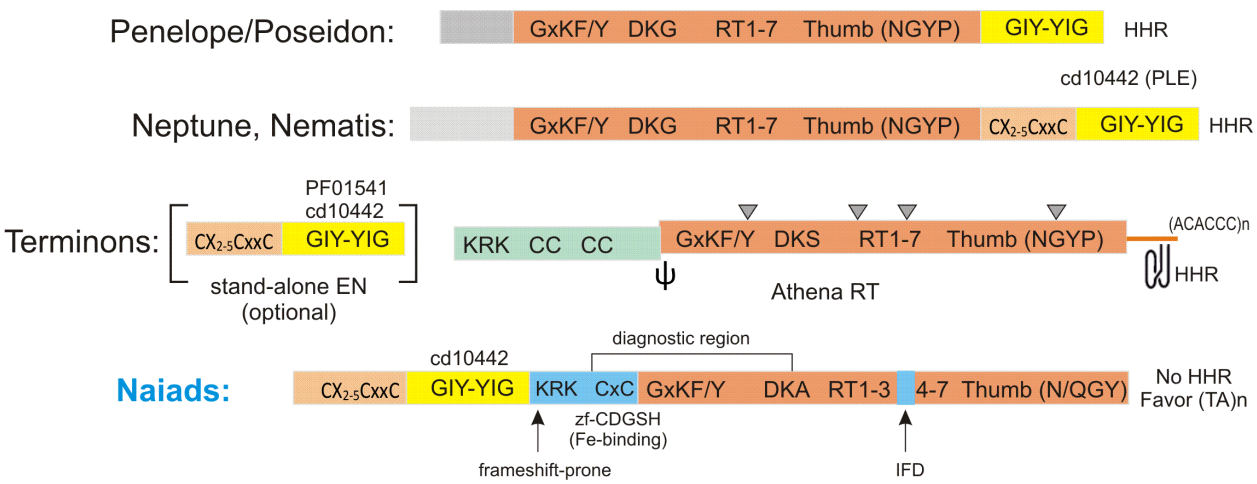

136
137

138 **Fig. 1**. Domain architecture of the major PLE types found in animals. Domains are colored as follows: RT
139 (peach), GIY-YIG (yellow), ORF1 (pink) often separated by a frameshift and a pseudoknot (ψ), Zn-fingers
140 (sand), and N-terminal domains with no characteristic motifs (gray). The organization of *Coprina* elements
141 from fungi, protists and plants is similar to *Athena*. *Naiad*-specific domains are in blue. CC, coiled-coil;
142 IFD, insertion in fingers domain; HHR, hammerhead ribozyme motif (also present in pLTRs of canonical
143 EN+ PLEs); KRK, nuclear localization signal; $(ACACCC)_n$, short stretches of reverse-complement
144 telomeric repeats in EN-deficient PLEs. Conserved introns are denoted by triangles. Also shown are the
145 most conserved amino acid motifs and the highest-scoring PFAM/CD domain matches. Not to scale.

146

147 ***Structural characteristics of Naiad elements***

148

149 Structurally, *Naiad* insertions exhibit most of the previously known characteristic
150 features of PLEs (Evgen'ev and Arkhipova 2005; Arkhipova 2006). Insertions show a
151 high degree of 5'-truncation and are often organized into partial tandems, so that a full-
152 length copy would be preceded by a partially truncated copy, forming a pLTR. Often,
153 there is also an inverted 5'-truncated copy found immediately adjacent at the 5'-end,
154 leading to formation of inverted repeats flanking the entire insertion unit (Fig. 2). Such
155 complex structures of insertions often lead to problems in WGS assembly, especially
156 short read-based. To further complicate boundary recognition, a 30-40 bp extension
157 ("tail") is usually found at either end of the insertion unit, most likely resulting from EN-
158 mediated resolution of the transposition intermediate. However, a notable difference
159 between *Naiads* and canonical PLEs is the absence of any detectable hammerhead
160 ribozyme motifs (HHR), which are typically located within pLTRs (Cervera and De la
161 Peña 2014; Arkhipova, et al. 2017). Ignoring any tandemly inserted sequence, the main
162 body of full-length *Naiad* copies are generally 3.4 - 4.4 kb.

163

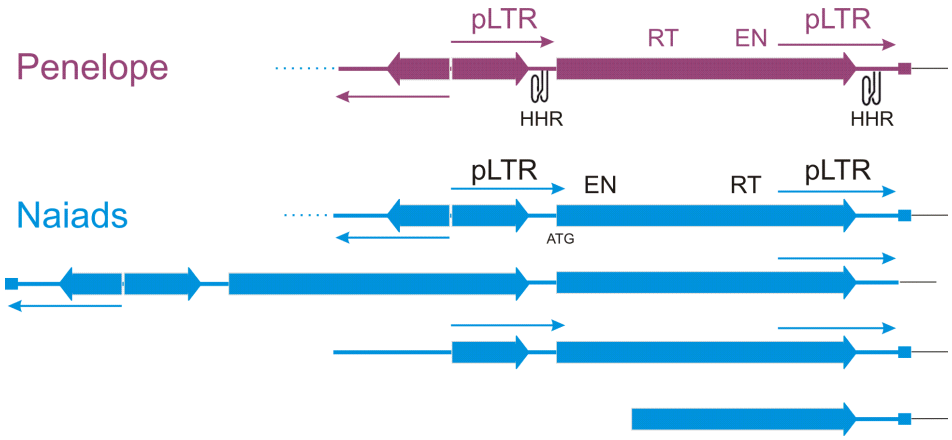

164
165

166 **Fig. 2**. Structural arrangements of PLE copies. Shown is the typical arrangement of two or more ORFs in
167 partial tandems, forming pseudo-LTRs (pLTRs) denoted by arrows. An inverted 5'-truncated copy is often
168 found adjacent to the upstream pLTR, forming an inverted-repeat structure. A small square denotes a 30-
169 40 bp extension ("tail") that is usually present only on one end of the insertion. HHR, hammerhead
170 ribozyme motif. For *Penelope*, only the most typical structure is shown, but all other variants also
171 observed.

172 Sequence conservation of the RT domain is strong enough to retrieve RTs of canonical
173 PLEs in a BLAST search, thus it is practical to rely on several diagnostic regions, such
174 as the CxC motif (showing weak homology to zf-CDGSH Fe-binding Zn-fingers) and the
175 DKG motif (Arkhipova 2006), which in *Naiads* is modified to DKA (Fig. 1). In the core
176 RT, the region between RT3(A) and RT4(B) is ~20 aa longer than in other PLEs and
177 corresponds in position to the IFD (insertion in the fingers domain) of TERTs (Lingner,
178 et al. 1997; Lue, et al. 2003) (Fig. S1). Interestingly, the IFD is missing from *Naiads* in
179 chelicerates (spiders and the horseshoe crab) and *D. stevensoni*, which resemble
180 canonical PLEs in this region. Finally, between RT and the upstream EN domain there
181 is usually a large KR-rich block harboring a nuclear localization signal (Fig. 3B). This
182 block, which is rich in adenines, is particularly prone to frameshift mutations resulting in
183 detachment of the EN domain from RT and its eventual loss. Such mutations apparently
184 prevented earlier recognition of the EN domain in *C. gigas* and *E. texana* PLEs from
185 Repbase (Bao, et al. 2015).
186
187 The EN domain in *Naiads* displays most similarity to the GIY-YIG EN of other PLEs
188 (cd10442), especially those in the *Neptune* and *Nematis* clades which harbor an
189 additional conserved $CX_{2-5}CxxC$ Zn-finger-like motif (lengthened by 5-aa insert in
190 mussels) upstream from the GIY-YIG motif (Fig. 1, 3A, S2). Perhaps it may facilitate
191 recognition of $(TA)_n$ microsatellite sequences, which often serve as preferred targets for
192 *Naiad* insertion. Its designation as a Zn-finger is tentative, as it shows variably non-
193 significant matches to ZnF_NFX, ZnF_A20, ZnF_TAZ, ZnF_U1 or RING fingers in
194 SMART database searches (Letunic, et al. 2020). The CCHH Zn-finger-like motif with
195 two cysteines inside the GIY-YIG core, characteristic of all canonical EN+ PLEs
196 (Arkhipova 2006), is also present, and the catalytic domain beyond the GIY-YIG core is
197 well conserved and includes the R, H, E and N residues implicated in catalysis (Van
198 Roey, et al. 2002). Thus, despite the permuted arrangement of the RT and EN domains,
199 *Naiads* share the peculiarities of structural organization with other PLEs, indicating that
200 their retrotransposition likely proceeds through a similar mechanism.
201

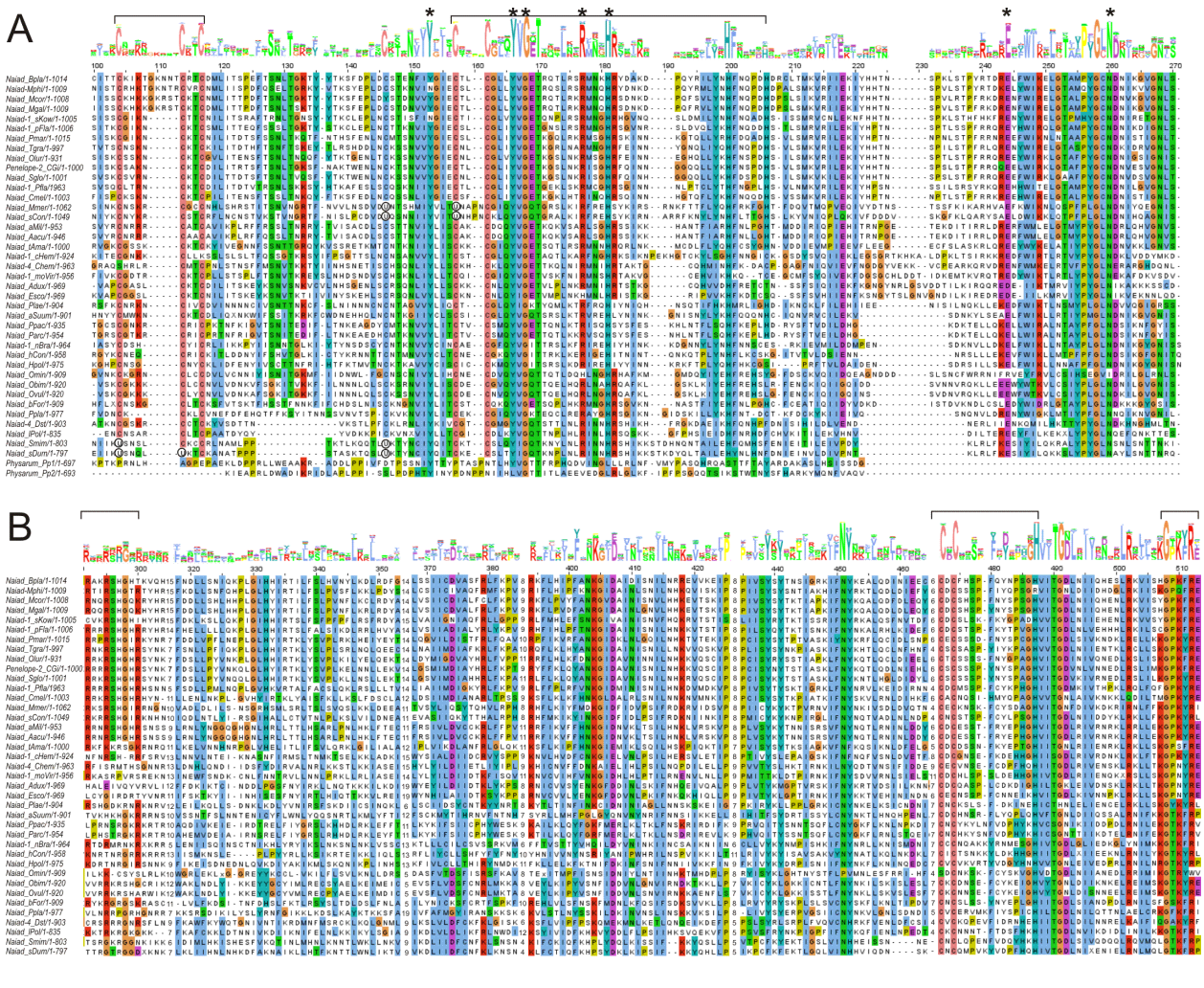

Fig. 3. Multiple sequence alignments of conserved domains characteristic for Naiads. (**A**) The GIY-YIG EN domain. The Zn-finger-like motifs are demarcated by square brackets; catalytic residues are denoted by asterisks; residues corresponding to selenocysteines (U) are circled. The position of the second His in the CCHH motif is variable. (**B**) The conserved diagnostic region between the EN domain and the GxKF/Y motif present in other PLEs. The KR-rich, CxC and GxKF/Y motifs are marked by square brackets. Alignments were visualized in Jalview and the sequence logos were created by AlignmentViewer (Waterhouse, et al. 2009; Gabler, et al. 2020), using the Clustal2 coloring scheme. The sequence order corresponds to that in Fig. 5.

Naiads can reach exceptionally high copy numbers

While PLEs in animal genomes are typically outnumbered by non-LTR and LTR retrotransposons, we noticed that *Naiads* can be particularly successful in certain

genomes in comparison to known PLE types. For example, inspection of TE landscape divergence profiles in the acanthocephalan *P. laevis* (Fig. 4A) shows that PLE families are responsible for 8.9% of the genome, of which *Naiad-1* occupies 7.8%. The remaining 12 *Neptune* and 4 *Penelope*/*Poseidon* families combined occupy only 1.1% of the genome (Fig. 4B).

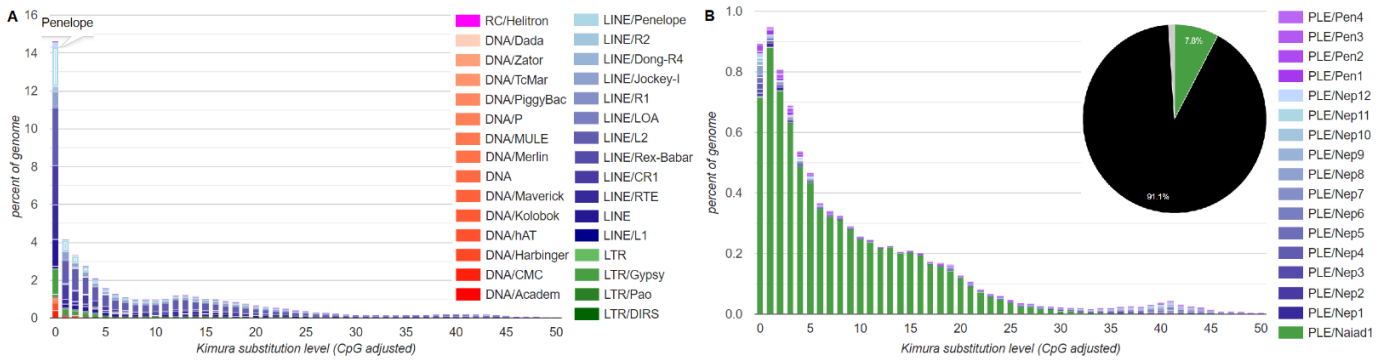

Fig. 4. Landscape divergence plots showing TE activity over time and genome occupancy in the acanthocephalan *Pomphorhynchus laevis*. (**A**) All TEs, with PLEs in light blue; (**B**) PLEs only, subdivided by families, with Naiad1_Plae family shown in green on the divergence plot and on the inserted pie chart.

We estimated copy numbers in each host species by querying each WGS assembly with the corresponding *Naiad* consensus sequence and counting the number of 3'-ends at least 80 bp in length. This approach avoids counting multiple fragments in lower-quality assemblies. Among hosts, significant variation in *Naiad* copy number can be observed, even between closely related species (Fig. 5). Copy numbers mostly reflect activity levels: some *Naiads* are apparently intact and are still successfully amplifying, while in other species they have been inactivated a long time ago and required numerous ORF corrections to yield an intact consensus. Surprisingly, several marine invertebrates, such as oysters, clams and crabs, harbor tens of thousands of *Naiad* copies, with nearly 37,000 in the blue crab *Paralithodes platypus*. The lack of HHR motifs obviously has not hampered the proliferative capacity of *Naiads*, as they can outnumber canonical HHR-bearing PLE families in the same species by several orders of magnitude, as in *P. laevis* (Fig. 4B).

241 It is also evident that the *Naiad* phylogeny does not necessarily parallel that of host
242 species. While some species, such as *Clytia hemisphaerica* or *D. stevensoni*, have
243 experienced substantial within-species *Naiad* diversification, harboring four families
244 each, others, such as hemichordates (*Saccoglossus kowalevskii*, *Ptychodera flava*), or
245 cephalopods (*Architeuthis dux, Euprymna scolopes*, and *Octopus spp*.), harbor families
246 belonging to different *Naiad* lineages (Fig. 5A). The fish *Naiads* (from *Chatrabus*
247 *melanurus, Thalassophryne amazonica* and *Eptatretus burgeri*) do not form a
248 monophyletic clade, while the nematode or arthropod *Naiads* do (Fig. 5A). The overall
249 distribution pattern is suggestive of vertical inheritance punctuated by occasional
250 horizontal transfer events and multiple losses.
251

252 ***Naiad selenoproteins in clams and spiders***

253

254 The ORFs of four *Naiads*, from two clams (*Sinonovacula constricta* and *Mercenaria*
255 *mercenaria*) and two spiders (*Stegodyphus dumicola* and *Stegodyphus mimosarum*),
256 each contained either three (*Naiad_Smim* and *Naiad_Mmer*) or four (*Naiad_sDum* and
257 *Naiad_sCon*) in-frame UGA codons. Except for one UGA codon in *Naiad_sCon*, all
258 UGA codons corresponded to highly conserved cysteines in the protein sequences of
259 other *Naiads* (Fig. 3). In all families, UGA codons corresponded to the cysteine
260 preceding the GIY-YIG motif, and the cysteine eight aa downstream of the DKA motif
261 (not shown). In spiders, UGA codons corresponded to either the first (*Naiad_Smim*) or
262 both the first and second (*Naiad_sDum*) cysteines in the $CX_{2\text{-}5}CxxC$ Zn-finger, while in
263 clams UGA codons corresponded to the first cysteine in the CCHH Zn-finger. The single
264 remaining UGA codon in *Naiad_sCon* corresponded to an aa in RT6(D) that was not
265 strongly constrained.
266

267 Given the correspondence between the in-frame UGA codons and conserved cysteines,
268 we hypothesized that the ORFs of these *Naiads* may encode selenoproteins, in which
269 UGA is recoded from stop to selenocysteine (Sec). Recoding is achieved through a *cis*-
270 acting selenoprotein insertion sequence (SECIS), a Sec-specific tRNA and additional
271 *trans*-acting proteins (Berry, et al. 1991; Tujebajeva, et al. 2000). In eukaryotes, SECIS

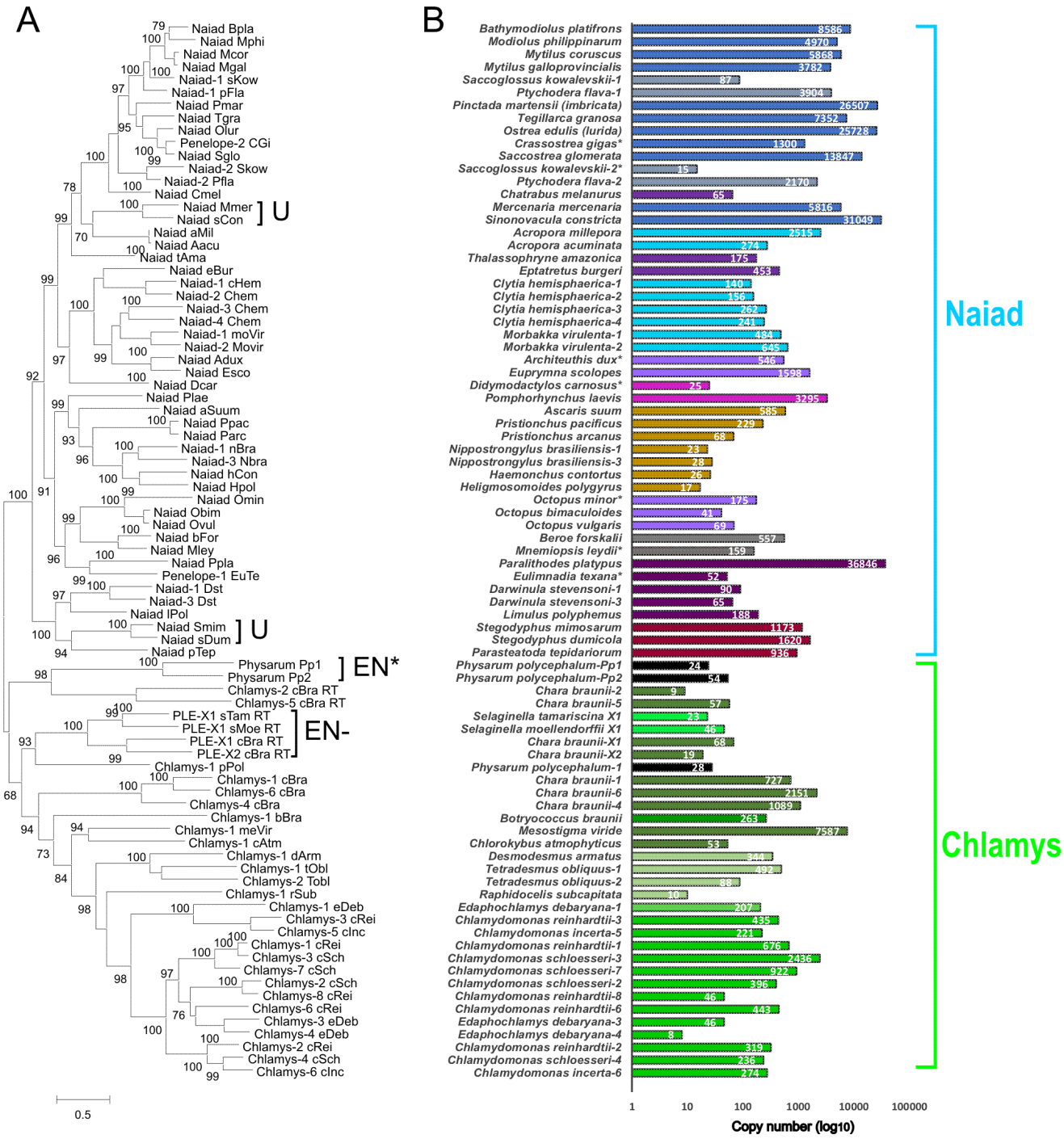

Fig. 5. Phylogenetic relationships between different *Naiad* and *Chlamys* families and copy number counts for each family. (**A**) The maximum likelihood phylogram shows branch support from 1000 ultrafast bootstrap replications. Families harboring selenocysteines are denoted by U, families lacking the EN domain by EN-, and families with EN remnants by EN*. Scale bar, aa substitutions per site. (**B**) The copy number chart displays counts for each family on a log scale. Similar colors denote similar taxonomic affiliations. Asterisks mark truncated or interrupted ORFs which are presumably non-functional.

280 elements are located in the 3' UTRs of selenoprotein mRNAs (Low and Berry 1996).
281 Using SECISearch3 (Mariotti, et al. 2013) to query each consensus sequence, we
282 identified "grade A" (i.e., the highest confidence) type I SECIS elements in all four of the
283 families (Fig. S3A). Except for *Naiad-Mmer*, the predicted SECIS elements were located
284 immediately downstream of the inferred UAA or UAG stop codons (1 – 21 bp
285 downstream, Fig. S3B), presumably placing the SECIS elements within the 3' UTRs of
286 each family. In *Naiad-Mmer*, the SECIS overlapped the first non-UGA stop codon,
287 however there was a UGA codon 7 bp upstream of the SECIS. The recoding of UGA is
288 position dependent (Turanov, et al. 2013) and a UGA codon in such close proximity to
289 the SECIS is not expected to efficiently encode Sec (Wen, et al. 1998), suggesting that
290 this UGA codon may function as stop in *Naiad-Mmer*. Overall, the ORFs of each of the
291 four families apparently encode selenoproteins that incorporate multiple Sec residues.
292 Furthermore, following the phylogenetic relationship of *Naiads* presented in Fig. 5A, it is
293 likely that the evolutionary transition to selenoproteins has occurred independently in
294 spiders and clams.
295

296 ***Structurally diverse Chlamys elements in the green lineage and protists***

297

298 As part of a recent annotation of TEs in the unicellular green alga *Chlamydomonas*
299 *reinhardtii* and its close relatives (Craig, et al. 2021), we identified novel PLE families
300 with N-terminal GIY-YIG domains. These elements were termed *Chlamys*, although
301 they were not further described. As with *Naiads*, the N-terminal EN+ PLEs in
302 *Chlamydomonas* possess several of the defining features of canonical C-terminal EN+
303 PLEs, including genome-wide distributions, frequent 5' truncation and partial tandem
304 insertions producing pLTRs. As introduced in the following text, *Naiad* and *Chlamys*
305 share several features and collectively form a strongly supported N-terminal EN+ clade
306 (Fig. 5A, Fig. 8), although *Chlamys* elements also possess characteristics that
307 distinguish them from the newly described metazoan clade.
308

309 The predicted proteins of the *Chlamys* elements included the *Naiad*-specific CxC zf-
310 CDGSH-like Zn-finger motif and the IFD (Fig. S1, S4). Additionally, all but two *Chlamys*

311 elements (*Chlamys-2_cBra* and *PLE-X1_cBra*) lacked HHRs, further strengthening their
312 evolutionary link to *Naiads*. As before, we used these conserved features to perform an
313 extensive search for related PLEs in other taxa. We curated *Chlamys* elements from a
314 wide diversity of green algae, including species from the Chlorophyceaen order
315 Sphaeropleales and the unicellular streptophyte algae *Mesostigma viride* and
316 *Chlorokybus atmophyticus*. The Sphaeropleales and Chlamydomonadales are
317 estimated to have diverged in the pre-Cambrian, while chlorophytes and streptophytes
318 (which includes land plants) possibly diverged more than 1 billion years ago (Del
319 Cortona et al., 2020). Additional curation identified more distantly related and
320 structurally diverse families in the chlorophyte *Botryococcus braunii* (class
321 Trebouxiophyceae), the multicellular streptophyte alga *Chara braunii*, two species of
322 spike moss (genus *Selaginella*) and the myxomycete slime mold *Physarum*
323 *polycephalum* (phylum Amoebozoa). Certain *Chlamys* families were also found in very
324 high copy numbers, most notably in the genomes of the streptophytes *M. viride* and *C.*
325 *braunii* (Fig. 5B).
326
327 *Chlamys* elements were mostly longer (3.3 – 8.2 kb, not including pLTRs) and more
328 structurally diverse than *Naiads* (see below). The length of several families was also
329 increased by the presence of tandem repeats. In the RT domain, the "DKG" motif was
330 present as DK without a well-conserved third aa, and the IFD was generally longer
331 (~20-40 aa) than that of *Naiads* (Fig. S1, S4). Targeted insertion at $(CA)_n$ repeats was
332 observed for many *Chlamys* elements. Relative to *Naiads*, the most striking difference
333 was in the EN domain. Although the GIY-YIG EN is N-terminal in both *Chlamys* and
334 *Naiads*, in *Chlamys* both the linker domain harboring the $CX_{2-5}CxxC$ Zn-finger and the
335 CCHH Zn-finger motif are absent (Fig. S2). Thus, the EN of *Chlamys* differ from both
336 *Naiads* and canonical C-terminal EN+ PLEs (all of which encode the CCHH motif, with
337 the $CX_{2-5}CxxC$ Zn-finger absent in *Penelope/Poseidon*). The conserved R, H, E and N
338 aa beyond the GIY-YIG core are all present in *Chlamys*. Finally, *Naiads* formed a well-
339 supported clade to the exception of all *Chlamys* elements (Fig. 5A). Collectively, *Naiad*
340 and *Chlamys* are distinguished based on both taxonomic and structural features, and

341 they can be considered as two major ancient groups that together comprise a wider N-
342 terminal EN+ clade.
343
344 The minimal *Chlamys* domain organization, which is shared by most families in
345 *Chlamydomonas,* the Sphaeropleales and the unicellular streptophytes, is represented
346 by *Chlamys-1_meVir* in Fig. 6. Five families from *Chlamydomonas* encoded proteins
347 with plant homeodomain (PHD) finger insertions, which were either located between
348 RT2a and RT3(A) (Fig. 7) or between the H and E conserved aa within EN. PHD fingers
349 have been reported from TEs including *CR1* non-LTR elements (Kapitonov and Jurka
350 2003) and *Rehavkus* DNA transposons (Dupeyron, et al. 2019), where they may play a
351 role in chromatin restructuring. PHD fingers are present in several other
352 retrotransposons and DNA transposons in *C. reinhardtii*, and it appears to be a common
353 accessory domain (Perez-Alegre, et al. 2005; Craig 2021). Several additional domains
354 were encoded by the more distantly related *Chlamys* elements. Two divergent
355 organizations were observed in *P. polycephalum* families, the first of which included an
356 SAP domain inserted between RT7(E) and the RT thumb (*Chlamys-1_pPol*, Fig. 6).
357 SAP (SAF A/B, Acinus and PIAS) is a putative DNA-binding domain that has previously
358 been reported in *Zisupton* DNA transposons (Böhne, et al. 2012). The second type
359 included the element *Physarum_Pp1,* which was first described from a 5' truncated
360 consensus as an unusual PLE with an IFD (Gladyshev and Arkhipova 2007). Extending
361 the consensus sequence revealed a predicted protein with a reduced N-terminus that
362 entirely lacked the CxC motif present in all other *Chlamys* and *Naiad*, and included a
363 reduced EN domain in which the GIY-YIG motif was present but weakly conserved and
364 the region containing the conserved R, H, E and N aa was absent (Fig. 3A, 6). Although
365 the *P. polycephalum* genome is highly fragmented, *Physarum_Pp1* does appear to be
366 present genome-wide.
367
368 EN+ PLEs were reported from the *C. braunii* genome project, although Nishiyama, et al.
369 (2018) did not further describe these elements. We observed three distinct types of
370 *Chlamys* in *C. braunii*. The first possessed long ORFs (~1,800 aa) encoding peptides
371 with a C-terminal extension including a motif with weak homology to Josephin and a

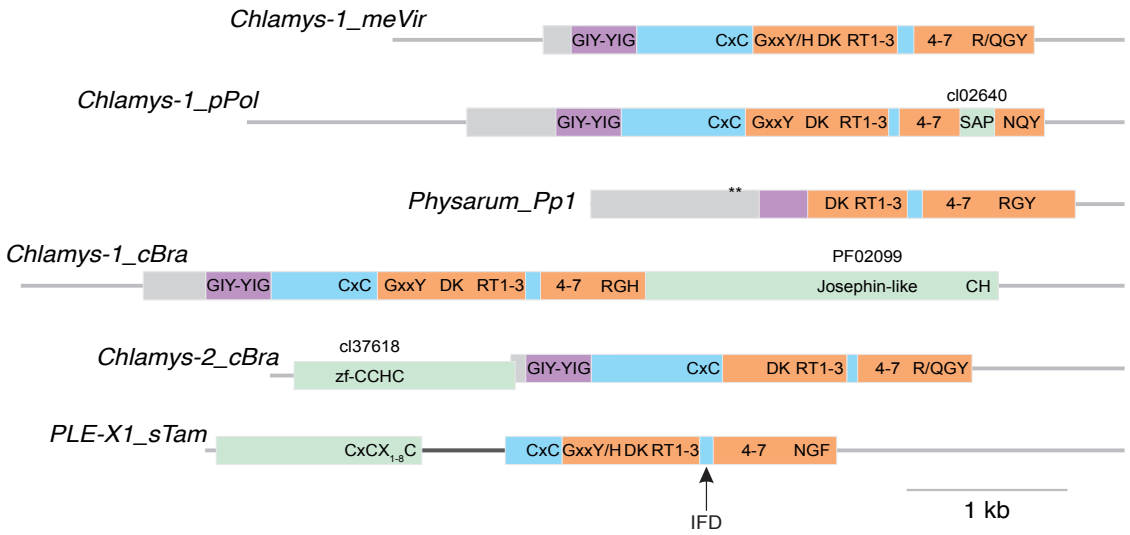

Fig. 6. Structural diversity of *Chlamys* elements. Domain architecture of *Chlamys* elements is represented by to scale schematics. Thin gray lines represent sequences not present in ORFs. Domains are colored as follows: RT, peach; GIY-YIG EN, purple; insertions/extensions containing conserved motifs, green; N-terminal extensions without recognized domains, gray; regions specific to *Naiad* and *Chlamys*, light blue. Purple is used for the GIY-YIG EN to distinguish the *Chlamys* EN from the *Naiad* EN, which contains the CCHH motif and is represented in yellow in Fig. 1. The most conserved amino acid motifs and the highest-scoring PFAM/CD domain matches are also shown. The asterisks on the *Physarum_Pp1* model represent in-frame stop codons, which may indicate the presence of an undetected intron. Note the *Physarum_Pp1* EN-like domain is also reduced and weakly conserved (Fig. 3A). The dark gray line in *PLE-X1_sTam* represents an intron that was inferred from *S. moellendorffii* annotated gene models.

second motif with several well-conserved C and H aa (*Chlamys-1_cBra*, Fig. 6). Josephin-like cysteine protease domains are present in *Dualen* non-LTR elements, where they may play a role in disrupting protein degradation (Kojima and Fujiwara 2005). The second type included an upstream ORF encoding a peptide with a gag-like zinc-knuckle domain (zf-CCHC, *Chlamys-2_cBra*, Fig. 6). The third type was notable since related elements were also identified in spike mosses, and a small number of highly significant BLASTp results were recovered from moss species, potentially indicating a wider distribution in “early-diverging” plants. These families include the CxC motif but lack the GIY-YIG EN, with a unique N-terminal extension that is likely separated by an intron and includes a conserved $CxCX_{1\text{-}8}C$ motif (*PLE-X1_sTam*, Fig. 6). The families in *C. braunii* appeared to have genome-wide distributions, and

395 remarkably, the two spike moss families exhibited targeted insertions at a precise
396 location within 28S ribosomal RNA genes. The insertion target differed by only 4 bp
397 between the families (Fig. S5), suggesting deep conservation of the target sequence at
398 least since the divergence of *S. moellendorffii* and *S. tamariscina* ~300 Mya (Xu, et al.
399 2018). Metazoan ribosomal DNA is a well-documented insertion niche for *R* element
400 non-LTRs and the *piggyBac* DNA transposon *Pokey* (Eickbush and Eickbush 2007),
401 although to our knowledge this is the first example from both plants and PLEs. It
402 remains to be seen how this group achieve either genome-wide or targeted ribosomal
403 DNA insertion without an identified EN. Interestingly, these families form a well-
404 supported clade with the EN+ family from *P. polycephalum* (*Chlamys-1_pPol*, Fig. 5A),
405 potentially indicating secondary loss of the GIY-YIG EN.
406

407 ***Functional characterization of an active Chlamys element***

408

409 As high-quality functional data is available for *C. reinhardtii*, we further focused on the
410 10 *Chlamys* families curated in this species. Notably, we also identified putatively
411 nonautonomous *Chlamys* elements, which produced pLTRs (and often multi-copy head-
412 to-tail insertions) and generally exhibited sequence similarity to autonomous families at
413 their 3' ends. The nonautonomous elements include *MRC1*, which was previously
414 described as a nonautonomous LTR (Kim, et al. 2006) and may be the most active TE
415 in *C. reinhardtii* laboratory strains (Neupert, et al. 2020). Further supporting recent
416 activity, *Chlamys* copies exhibited minimal divergence from their respective consensus
417 sequences (Fig. S6) and within-species polymorphic insertions were observed for
418 copies of all 10 autonomous families by comparison to a newly assembled PacBio-
419 based genome of the divergent field isolate CC-2931 (Supp. note). Cumulatively,
420 *Chlamys* PLEs spanned ~1.6% of the 111 Mb *C. reinhardtii* genome and comprised
421 ~15% of the total TE sequence.
422

423 Only one active C-terminal EN+ PLE has been experimentally characterized, the
424 archetypal *Penelope* of *D. virilis* (Pyatkov, et al. 2004; Schostak, et al. 2008). In an
425 attempt to characterize a *Chlamys* element, we searched for an actively transcribed

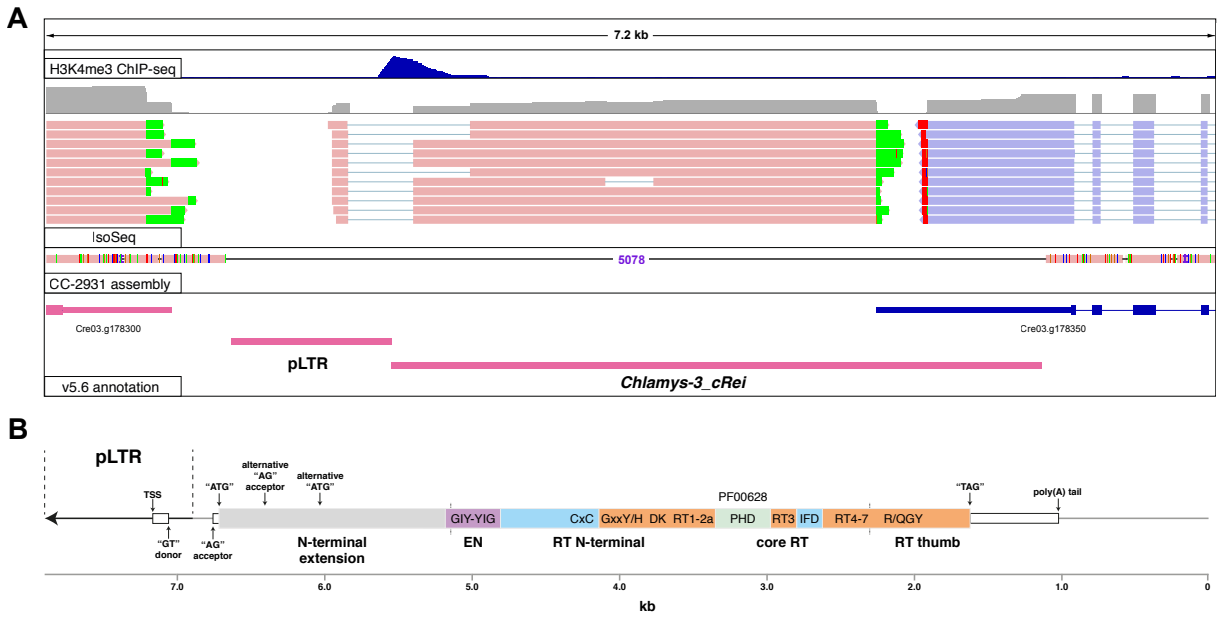

Fig. 7. Functional characterization of an active *Chlamys* element in *C. reinhardtii.* **(A)** IGV browser view (Robinson, et al. 2011) of a *Chlamys-3_cRei* copy that is polymorphic between the reference genome and the divergent field isolate CC-2931. Green and red mismatched bases on Iso-Seq reads represent poly(A) tails of transcripts. Forward strand reads and gene/repeat models are shown in pink, and reverse strand in blue. **(B)** Schematic of the inferred gene model and structural organization of *Chlamys-3_cRei*. Note that this represents the full-length element and the transcribed copy above contains a 2.84 kb internal deletion, the boundaries of which are shown by the dashed black lines. Domains are colored as in Fig. 6 and conserved motifs are textually represented as shown for *Chlamys-1_meVir* in that figure.

copy using recent PacBio RNA-seq (i.e. Iso-Seq) and H3K4me3 ChIP-seq datasets (Gallaher, et al. 2021), with the H3K4me3 modification reliably marking active promoters in *C. reinhardtii* (Ngan, et al. 2015). Due to frequent 5' truncation, only two families were found with full-length copies, and transcription was observed for only a single copy of the *Chlamys-3_cRei* family (Fig. 7A). Unfortunately, this copy features a 2.8 kb deletion, although this is entirely within the ORF and the copy presumably retains a functional promoter, transcription start site (TSS) and terminator. Strikingly, the derived gene model of *Chlamys-3_cRei* (Fig. 7B) shared several features with *Penelope*, in which the pLTR harbors the TSS and a 75 bp intron within the 5' UTR that overlaps the internal promoter (Arkhipova, et al. 2003; Schostak, et al. 2008). In *Chlamys-3_cRei*, the TSS is also located in the pLTR and a 398 bp intron within the 5' UTR spans the boundary between the pLTR and downstream main body. The H3K4me3 ChIP-seq supports an

internal promoter coinciding with the intron. Additionally, three Iso-Seq reads supported an alternative isoform with a 751 bp intron. This isoform initiates at a downstream start codon and results in a peptide truncated by 293 aa, although as the predicted *Chlamys-3_cRei* peptide includes an N-terminal extension both isoforms encode complete EN and RT domains. The similarities between *Penelope* and *Chlamys-3_cRei* potentially indicate an ancient and deeply conserved organization and perhaps mechanism shared by canonical PLEs and the N-terminal EN+ PLEs described herein.

Hydra: A novel C-terminal EN+ clade

While performing an updated phylogenetic analysis of all PLEs (see below), we noticed that seven C-terminal EN+ families in Repbase formed an isolated group highly divergent from *Neptune, Penelope/Poseidon* and *Nematis*. All but one of these families were annotated from the freshwater polyp *Hydra magnipapillata*. Using protein homology searches, we identified a small number of additional families in other aquatic invertebrates spanning four phyla (Cnidaria, Mollusca, Echinodermata, and Arthropoda), notably in species such as the stony coral *Acropora millepora* and the sea cucumber *Apostichopus japonicus*. These elements were generally short (<3 kb) and contained single ORFs encoding peptides with several similarities to canonical C-terminal EN+ PLEs, i.e. no CxC motif, no IFD and a C-terminal GIY-YIG EN (Fig. S7). HHRs were also detected, strengthening the relationship with canonical PLEs. However, these families also exhibited unique features. The N-terminal GxKF/Y motif was not well conserved, the DKG motif was modified to DKT, and RT4(B) was particularly divergent and challenging to align. Most notably, in the EN domain the CCHH motif universal to C-terminal EN+ PLEs (and *Naiads*) was absent (Fig. S2, S7). A linker domain was present which was most similar to that of *Nematis*, although the $CX_{2\text{-}5}CxxC$ Zn-finger was modified to a $CxCX_5C$ motif. Interestingly, all families exhibited insertions into $(TA)_n$, strengthening the association between the linker domain and targeted insertion. We name this new clade of C-terminal EN+ PLEs *Hydra*, in line with both their aquatic hosts and their discovery in *H. magnipapillata*.

479 ***Evolution of the RT and GIY-YIG EN domains***

480

481 As seen in Fig. 5, the newly discovered types of PLE span much of the well-sequenced
482 taxonomic diversity in Eukarya, including protists, plants, and animals. We placed
483 *Naiad, Chlamys* and *Hydra* representatives into a reference PLE dataset that included
484 the previously known EN+ *Penelope/Poseidon, Neptune, Nematis* and EN– *Athena* and
485 *Coprina* clades, as well as representatives of the sister clade to PLEs, the TERTs
486 (Arkhipova 2006; Gladyshev and Arkhipova 2007). The combined phylogeny of the
487 extended core RT domain, which also includes the RT thumb and the previously
488 identified N-terminal conserved motifs N1-N3 (Arkhipova 2006), is presented in Fig. 8.
489 With the exception of *Neptune*, all of the above clades were recovered with ultrafast
490 bootstrap support values >90%. The monophyly of *Neptune* was not recovered, with
491 *Neptune* elements forming a paraphyletic group in a weakly supported clade with the
492 taxonomically diverse EN– *Coprina* elements, as also occurred in a previous analysis
493 (Arkhipova, et al. 2017). The novel N-terminal EN+ elements (i.e. *Naiad* + *Chlamys*)
494 formed a strongly supported clade, although *Chlamys* was paraphyletic with respect to
495 the *Naiad* clade and the internal topologies of the more structurally diverse *Chlamys*
496 elements were not well supported. Despite its potential paraphyly, we still consider
497 *Chlamys* to be a useful grouping given its unique structural features. The rotifer-specific
498 EN– *Athena* elements formed the most basal PLE clade when rooting the phylogeny on
499 TERTs, although the deep branches linking the major PLE clades generally received
500 weak support. As seen in both *Chlamys* and *Neptune*, EN– families occasionally
501 emerge within EN+ clades, apparently as a result of EN loss accompanied by
502 acquisition of an alternative way of employing accessible 3'-OH ends for RT priming.
503 Overall, it is evident that, with inclusion of the hitherto unknown superfamilies, PLE RTs
504 display an astonishing level of clade diversity, which is comparable to that of non-LTR
505 and LTR retrotransposon RTs, and will undoubtedly increase in line with the number of
506 sequenced genomes from under-represented eukaryotic branches of the tree of life.

507

508

509

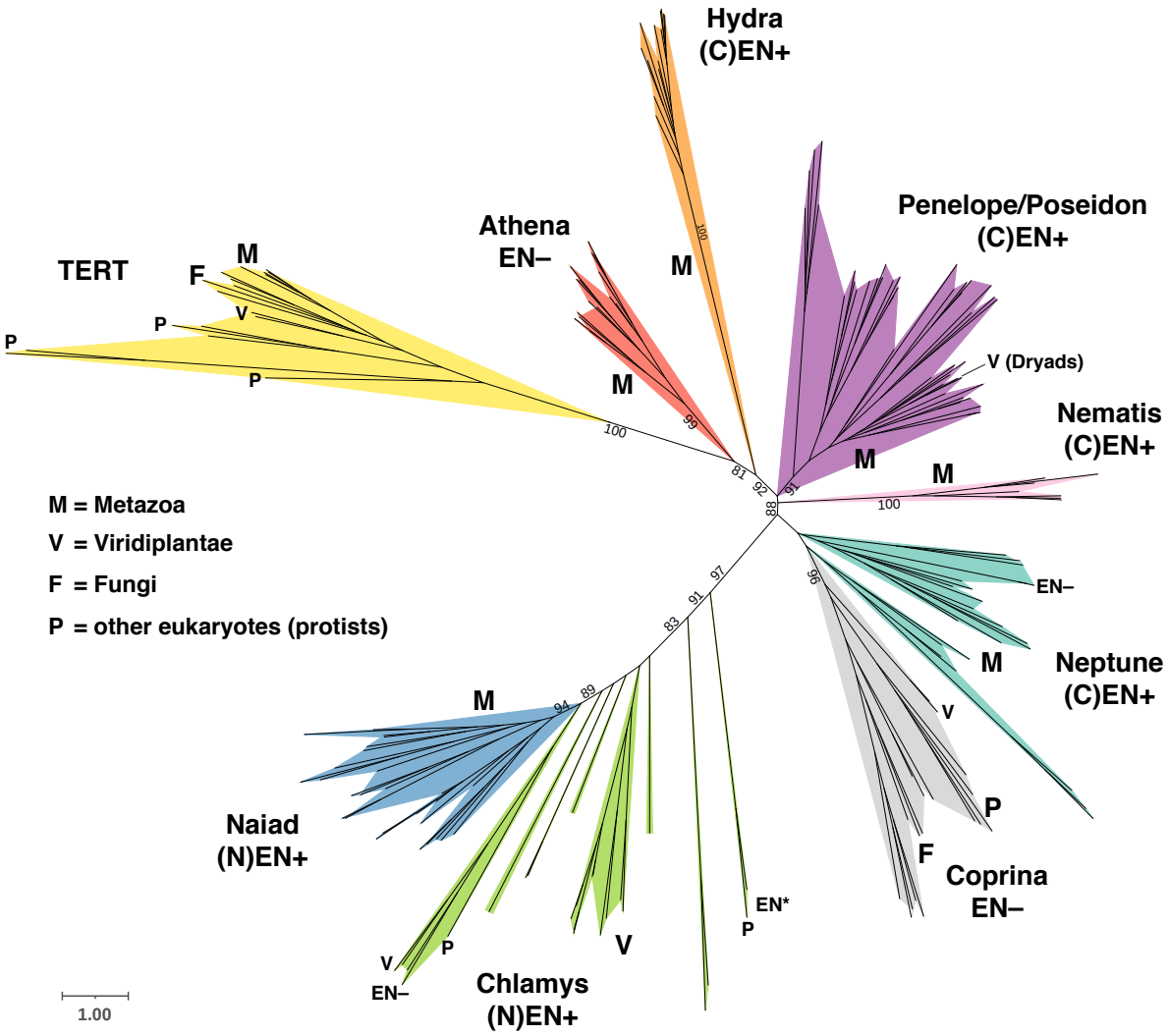

Fig. 8. Core RT maximum likelihood phylogeny of PLE RTs and TERTs. Support values from 1000 ultrafast bootstrap replications are shown, with all values from nodes within major clades (colored) and any values <70 at deeper nodes excluded to aid visualization. The taxonomic range of clades and subclades is shown by letters. Note that the "V" marking the "*Dryad*" subclade within *Penelope/Poseidon* points at three conifer families from the presumed horizontal transfer event (Lin, et al. 2016). The location of EN in EN+ groups is provided by the prefixes (N) and (C) for N-terminal and C-terminal, respectively. Subclades with EN remnants or no EN that are within EN+ clades are shown by EN* and EN– tags, respectively. Scale bar, aa substitutions per site. The phylogeny was annotated using iTOL (Letunic and Bork 2019).

523 In light of the increased diversity uncovered by *Naiad, Chlamys* and *Hydra* PLEs, we
524 also attempted to further elucidate the evolutionary relationships of the GIY-YIG EN
525 domain. Since the domain is too short for conventional phylogenetic analysis, it has
526 previously been analyzed using protein clustering approaches. Dunin-Horkawicz, et al.
527 (2006) found that the most similar ENs to those from canonical C-terminal EN+ PLEs
528 belonged to the HE_Tlr8p_PBC-V_like group (cd10443), which includes homing ENs
529 from bacteria, chloroviruses (e.g. *Paramecium bursaria* chlorella virus 1, PBCV-1) and
530 iridoviruses, as well as an EN from the *Tlr8* Maverick/Polinton element from
531 *Tetrahymena thermophila*. Using CLANS (Frickey and Lupas 2004), we performed an
532 updated clustering analysis with all available PLE ENs (Fig. S8). *Neptune, Nematis* and
533 *Penelope/Poseidon* ENs formed distinct although strongly connected clusters, with
534 *Naiad* ENs essentially indistinguishable from *Neptune*. These results largely follow
535 expectations from the shared presence of the CCHH motif and the presence/absence of
536 the CX_{2-5}CxxC Zn-finger linker (Fig. S2), and these domains are collectively
537 representative of the canonical PLE EN described in NCBI (cd10442). *Hydra* ENs
538 formed a distinct and well-resolved cluster that was nonetheless related to other PLE
539 ENs, in line with the absence of the CCHH motif and the alternative configuration of the
540 linker motif. Interestingly, the ENs sometimes associated with the giant *Terminons* (Fig.
541 1), which contain RTs from the otherwise EN– *Athena* group (Arkhipova, et al. 2017),
542 were also recovered as a distinct cluster related to other PLE ENs. These ENs include
543 both the CX_{2-5}CxxC and CCHH motifs, suggesting shared ancestry with EN+ PLEs,
544 although they also contain large unique insertions (Fig. S2). Finally, the *Chlamys* ENs
545 were diffusely clustered between all other PLE ENs and several ENs from the
546 HE_Tlr8p_PBC-V_like group. The lack of strong clustering can likely be explained by
547 the lack of both the CX_{2-5}CxxC and CCHH motifs resulting in fewer conserved sites, and
548 the possible link between *Chlamys* and HE_Tlr8p_PBC-V_like ENs should be
549 interpreted tentatively. Overall, the GIY-YIG ENs of all PLEs appear to be related, and
550 in line with the results of Dunin-Horkawicz, et al. (2006), PLE ENs are most similar to
551 particular homing ENs from bacteria and viruses.
552
553

554 **DISCUSSION**

555

556 ***A new major PLE clade with N-terminal EN and its impact on genome and***
557 ***transposon annotation***

558

559 *Penelope*-like elements are arguably the most enigmatic type of retrotransposable
560 elements inhabiting eukaryotic genomes. Due to their absence from the best-studied
561 genomes such as mammals, birds and angiosperms, and the complex tandem/inverted
562 structures brought about by still undefined features of their peculiar transposition cycle,
563 PLEs have largely been neglected and overlooked by most computational pipelines
564 used in comparative genomics. Current approaches distinguish PLEs by the presence
565 of a PLE-related RT, and classify them to the "order" level as a clade of non-LTR
566 elements (Bao, et al. 2015) without subdivision into groups differing by domain
567 architecture and phylogenetic placement, as is commonly done for non-LTR (LINE) and
568 LTR retrotransposons (Storer, et al. 2021). Here we show that the degree of PLE
569 structural and phylogenetic diversity matches that of non-LTR and LTR
570 retrotransposons, emphasizing the need for updating current classification schemes and
571 TE-processing computational pipelines.

572

573 Our data also underscore the need to adjust computational pipelines to incorporate
574 searches for GIY-YIG EN either upstream or downstream from PLE RT, due to the high
575 degree of polymorphisms (especially frameshifts) in the connector region, which
576 complicates identification of full-length elements. This is especially relevant at a time
577 when increasing numbers of invertebrate genomes are being sequenced, with *Naiad*
578 elements often contributing tens of thousands of copies to metazoan genomic DNA.
579 Under-annotation of poorly recognizable TEs poses a serious problem to gene
580 annotation. This is especially well-illustrated in host-associated and environmental
581 metagenome analyses, where understudied eukaryotic TEs become mis-assigned to
582 bacterial genomes and are propagated in taxonomy-aware reference databases,
583 jeopardizing future automated annotations (Arkhipova 2020).

584 Of special interest is the dominance of *Chlamys* PLEs in the plant kingdom, where their
585 ancient nature is supported by their presence in the most basal members of the green
586 lineage, by a high degree of divergence between *Chlamys* elements, and by distinctive
587 features of the associated EN. In contrast to the documented case of horizontal transfer
588 of a canonical C-terminal EN+ PLE into conifer genomes (Lin, et al. 2016), their early-
589 branching position in the PLE phylogeny argues that they constitute ancestral genome
590 components in early-branching plants and green algae, and does not support recent
591 introduction. Nevertheless, their ongoing activity and diversification in *Chlamydomonas*
592 indicates that *Chlamys* elements are actively participating in algal genome evolution.
593
594 ***Common and distinctive features of Naiad* and *Chlamys retrotransposition***
595
596 Consistent association of all PLE RTs with a special type of endonuclease/nickase
597 (GIY-YIG EN), which may have occurred several times in early eukaryotic evolution to
598 form distinct lineages characterized by N- or C-terminal EN domains, underscores the
599 importance of this EN for efficient intragenomic proliferation mediated by PLE RT, and
600 emphasizes the need for further mechanistic investigations of the non-trivial PLE
601 transposition cycle in representatives of each PLE lineage. It is very likely that the
602 unique EN cleavage properties determine the formation of complex tandem/inverted
603 pLTRs and the “tail” extension on either side of PLEs, not observed during TPRT of
604 non-LTR elements, but seen in *Naiad/Chlamys*.
605
606 Further, PLEs are highly unusual among retroelements in their ability to retain introns
607 after retrotransposition, sometimes even retrotransposing intron-containing host genes
608 *in trans* (Arkhipova, et al. 2003; Arkhipova, et al. 2013). While most of the
609 *Naiad/Chlamys* ORFs are not interrupted by introns, the functionally characterized
610 active *Chlamys-3_cRei* element shares an intron position within the 5’-UTR with the
611 functionally studied *Penelope* from *D. virilis*, overlapping with the internal promoter
612 (Schostak, et al. 2008). This suggests that other PLEs may share this organization and
613 harbor introns upstream of the main ORF. The significance of intron retention is

614 unknown, although it is likely a consequence of the unusual retrotransposition
615 mechanism.
616
617 Interestingly, we did not detect HHR motifs in *Naiad* or *Chlamys* elements, except for
618 *Chlamys-2_cBra* (EN+) and *PLE-X1_cBra* (EN–). These two families from *C. braunii* are
619 not closely related (Fig. 5A), implying HHRs may have been independently acquired or
620 frequently lost from other *Chlamys*. Conversely, HHRs are universally present in the
621 *Hydra* clade and other PLEs. HHR function in EN+ PLEs is still unclear, and while they
622 have been hypothesized to help cleave the tandemly arranged long precursor RNAs
623 (Cervera and De la Peña 2014), their absence from *Naiads* and most *Chlamys*
624 elements obviously does not interfere with their successful intragenomic proliferation.
625
626 In many cases, it was not possible to discern target-site duplications in *Naiads* and
627 *Chlamys* due to a strong insertion bias towards microsatellite repeats, with $(CA)_n$ most
628 commonly observed in *Chlamys* and $(TA)_n$ in *Naiads*. The CX_{2-5}CxxC EN linker was
629 hypothesized to mediate such bias in *Neptune* PLEs (Arkhipova 2006) and could do so
630 in *Naiads*, but its absence from *Chlamys* suggests that the novel CxC domain may also
631 play a role in targeting EN activity to specific DNA repeats. Also of interest are the EN–
632 "*PLE-X*" families from two species of spike moss, which are the first known TEs to
633 exhibit targeted insertion into the 28S ribosomal RNA gene in plants, as is observed in
634 certain non-LTRs and DNA transposons of arthropods and other animals (Eickbush
635 2002; Penton and Crease 2004; Gladyshev and Arkhipova 2009).
636
637 Finally, it is unknown what role the IFD may play in *Naiads* and *Chlamys*. In TERTs, the
638 IFD aids the stabilization of telomerase RNA (TER) and DNA during the extension of
639 telomeric DNA (Jiang, et al. 2018). The IFD domain in *Naiads* and *Chlamys* is shorter
640 than that of TERTs, and its loss from a specific *Naiad* subclade demonstrates that it is
641 not necessarily a functional requirement.
642
643 Establishment of an *in vitro* system to study PLE retrotransposition mechanisms would
644 be the next important task required to achieve full understanding of PLE-specific TPRT

645 features that distinguish them from LINEs, such as formation of complex
646 tandem/inverted repeat structures and microsatellite insertion bias.
647
648 ***Naiad selenoproteins***
649
650 The *Naiads* that encode selenoproteins are notable for two reasons. First, almost all
651 described selenoproteins include a single Sec, whereas the *Naiads* contain either three
652 or four. Baclaocos, et al. (2019) performed analysis of selenoprotein P (SelP), one of
653 the few selenoproteins including multiple Sec residues, finding that in bivalves SelP
654 contains the most Sec residues of any metazoan group, and that spider SelP proteins
655 contain a moderate number of Sec residues. Bivalves in particular are known for their
656 high selenium content (Bryszewska and Måge 2015), and it may be that the *Naiads*
657 represent cases of TEs adapting to their host cellular environments. However, even in
658 bivalves selenoproteins are incredibly rare (e.g. the pacific oyster selenoproteome
659 encompasses 32 genes (Baclaocos, et al. 2019)), suggesting a more specific role for
660 the incorporation of Sec in these families. Sec residues are involved in numerous
661 physiological processes and are generally found at catalytic sites, where in many cases
662 they have a catalytic advantage relative to cysteine (Labunskyy, et al. 2014). All but one
663 of the Sec residues in *Naiad* peptides correspond to highly conserved sites in the CX_{2-}
664 $_{5}$CxxC Zn-finger, CCHH Zn-finger and the DKA motif, and although the precise
665 physiological role of these motifs in PLEs is unknown, it may be that the incorporation of
666 Sec provides both a catalytic and evolutionary advantage.
667
668 Second, the *Naiad* families are the first described selenoprotein-encoding TEs. It is
669 currently unclear whether these represent highly unusual cases, although the fact that
670 they appear to have evolved independently in spiders and clams hints that other
671 examples may be found in the future. This has potential implications for TE annotation
672 in general, and selenoprotein-encoding TEs may have previously been overlooked in
673 taxa such as bivalves because of apparent stop codons. Additionally, this result may
674 provide insight into evolution of new selenoproteins. The transition from encoding Cys to
675 Sec is expected to be a complex evolutionary process, since a gene must acquire a

676 SECIS element and near-simultaneously undergo a mutation from TGT/TGC (encoding
677 Cys) to TGA (Castellano, et al. 2004). The insertion of TEs carrying SECIS elements
678 into the 3' UTRs of genes could provide a pathway for SECIS acquisition, especially for
679 TEs that undergo 5' truncation and may insert with little additional sequence. It remains
680 to be seen if the selenoprotein-encoding *Naiads*, or indeed any other TEs, have
681 contributed to the evolution of new selenoproteins in their host genomes.
682
683 ***Evolutionary implications for PLE origin and diversification***
684
685 As the branching order of major PLE clades diverging from TERTs is not exceptionally
686 robust, it may be difficult to reconstitute evolutionary scenarios which were playing out
687 during early eukaryogenesis. It is possible that an ancestral EN– PLE, similar to *Athena*
688 or *Coprina* but lacking the extended N-terminus, was present at telomeres (Gladyshev
689 and Arkhipova 2007) before undergoing either multiple domain fusions to give rise to
690 TERTs, or fusions with GIY-YIG EN, either at the N- or at the C-termini, to form the
691 contemporary *Naiad/Chlamys, Neptune, Nematis*, and *Penelope/Poseidon*
692 superfamilies capable of intrachromosomal proliferation.
693
694 There are several plausible evolutionary scenarios that could explain the observed EN
695 and RT diversity, and ENs may have been acquired or exchanged several times by
696 different PLE clades. It is possible that *Chlamys* elements acquired an EN without the
697 $CX_{2\text{-}5}CxxC$ and CCHH motifs from a homing EN from the HE_Tlr8p_PBC-V_like family,
698 and that the Zn-finger motifs were later gained by *Naiads*. ENs with both Zn-fingers
699 could then have been transferred from *Naiads* to the C-termini of EN– animal PLEs
700 (once or multiple times), giving rise to other EN+ clades. This scenario would imply that
701 the internal CCHH was then lost in *Hydra*, and the upstream linker domain was either
702 reduced (*Nematis*), reduced and modified (*Hydra*) or lost (*Penelope*/*Poseidon*).
703 Alternatively, an EN containing one or both Zn-fingers could have been independently
704 acquired by C-terminal EN+ PLEs (again once or multiple times) and exchanged with
705 *Naiads* replacing the *Chlamys*-like EN (or gained independently by *Naiads* from a
706 similar homing EN). This scenario would imply the existence of homing ENs with Zn-

707 finger motifs, which have not been found, however both the $CX_{2-5}CxxC$ and CCHH
708 motifs are present in the stand-alone ENs occasionally associated with *Terminons*. EN
709 acquisition, either at the N- or C-terminus, may have been facilitated if RT and EN were
710 brought in proximity either on a carrier virus or on a chimeric circular replicon allowing
711 permutation. Any combination of events in the above scenarios could of course explain
712 the observed diversity. Notably, early metazoans such as cnidarians exhibit the highest
713 PLE clade diversity, with *Poseidon, Naiad* and *Hydra* present in *H. magnipapillata* and
714 *Neptune, Naiad* and *Hydra* in the coral *A. millepora*, implying that the appropriate
715 conditions existed for either multiple exchanges or acquisitions of ENs. Finally, EN
716 losses are not unusual, and EN– elements can emerge within EN+ clades, as in
717 *Chlamys* PLE-X families in *Selaginella* and *Chara*, or the *Neptune*-like *MjPLE01* from
718 the kuruma shrimp *Marsupenaeus japonicus* (Koyama, et al. 2013), if they adopt
719 alternative means of securing 3'-OH groups for TPRT.
720
721 While the IFD domain may have been inherited by *Naiads/Chlamys* from a common
722 ancestor with TERTs, IFD-like regions are also found sporadically in *Coprina* elements,
723 arguing against its use as a synapomorphy. It is possible that the IFD has been lost
724 multiple times in different PLE clades, as demonstrated by its loss in some *Naiads*, or
725 gained independently in *Naiads/Chlamys* and *Coprina*. The presence/absence of HHR
726 motifs does not provide many clues either: while found in only two basal *Chlamys*-like
727 elements and absent from *Naiads*, they are present in all other PLEs, both EN+ and
728 EN–. As with newly described retrozymes, they may exploit autonomous PLEs for their
729 proliferation (Cervera and de la Peña 2020), or they could provide an unknown function.
730
731 Regardless of the exact sequence of events which led to PLE diversification in early
732 eukaryotic evolution, it is now clear that the diversity of PLE structural organization,
733 manifested in the existence of at least seven deep-branching clades (superfamilies)
734 differing by domain architecture and found in genomes of protists, fungi, green and red
735 algae, plants, and metazoans from nearly every major invertebrate and vertebrate
736 phylum, can no longer be overlooked and should be reflected in modern genomic
737 analysis tools. As more genomes from neglected and phylogenetically diverse lineages

738 become available, it is likely that the diversity of PLEs will continue to expand, further
739 supporting their increasingly important and unique position in TE biology and their
740 contribution to shaping the amazing diversity of eukaryotic genomes.

741

742 **MATERIALS AND METHODS**

743

744 ***Annotation and curation of PLE consensus sequences***

745

746 For general TE identification and annotation in metazoan genome assemblies (*D.*
747 *stevensoni, P. laevis*), we used TEdenovo from the REPET package (Flutre, et al. 2011)
748 to build *de novo* repeat libraries with default parameters. Although REPET-derived *de*
749 *novo* TE consensus sequences are automatically classified under Wicker's scheme
750 (Wicker, et al. 2007), we additionally used RepeatMasker v4.1.0 (Smit, et al. 2015) for
751 TE classification, detection and divergence plot building, using the initial TEdenovo
752 repeat library. To specifically illustrate the composition on PLE families in the *P. laevis*
753 genome, we used the corresponding consensus sequences of PLE families as a local
754 library for divergence plot building.

755

756 Initial *Chlamys* consensus sequences from *C. reinhardtii* and its close relatives
757 (*Chlamydomonas incerta*, *Chlamydomonas schloesseri* and *Edaphochlamys*
758 *debaryana*) were curated as part of a wider annotation of TEs in these species (Craig
759 2021; Craig, et al. 2021). Inferred protein sequences from the metazoan and algal
760 consensus models were then used as PSI-BLAST or tBLASTn (Camacho, et al. 2009)
761 queries to identify related *Naiad* and *Chlamys* PLEs in other species. PSI-BLAST was
762 run using NCBI servers to identify putative PLE proteins that had been deposited in
763 NCBI. tBLASTn was performed against all eukaryotic genome assemblies accessed
764 from NCBI on 2020/04/09. Assemblies with multiple significant hits were selected for
765 further curation, and where several related species had multiple hits the most
766 contiguous assemblies were targeted. A Perl script was used to collect the nucleotide
767 sequence of each tBLASTn hit from a given assembly, and the most abundant putative
768 PLEs in each species were subjected to manual curation. This was performed by

769 retrieving multiple copies by BLASTn, extending the flanks of each copy and aligning
770 the subsequent sequences with MAFFT v7.273 (Katoh and Standley 2013). The
771 multiple sequence alignment of each family was then visualized and manually curated
772 (removing poorly aligned copies, identifying 3' termini and pLTRs if present, etc.).
773 Consensus sequences were produced for each family and protein sequences were
774 inferred by identifying the longest ORF.
775
776 Copy number was estimated by performing BLASTn against the assembly using the
777 consensus sequence as a query. NCBI BLASTn optimized for highly similar sequences
778 (megablast) was used with cutoff E-value 1e-5. Whole-genome shotgun (wgs) datasets
779 were used for each species, with the best quality assembly used in case of multiple
780 isolates. In most cases, NCBI web interface was used to control for truncated and
781 deleted copies via graphical summary. If the maximum number of target sequences
782 (5000) was exceeded, wgs datasets were created using blastn_vdb from the SRA
783 Toolkit and searched with blastn 2.6.1+, or installed locally and searched with blastn
784 2.10.1+.
785
786 Novel *Hydra* families were identified and curated using the same approach as above.
787 Existing protein sequences from *H. magnipapillata* PLEs accessed from Repbase were
788 used as initial queries to search for related elements, alignments of which were then
789 manually curated and used to produce consensus sequences.
790
791 ***Functional motif identification***
792
793 SECIS elements were identified in *Naiad* consensus sequences containing in-frame
794 UGA codons using the SECISearch3 (Mariotti, et al. 2013) online server
795 (http://gladyshevlab.org/SelenoproteinPredictionServer/).
796
797 Hammerhead ribozyme motif (HHR) motif searches were performed using secondary
798 structure-based software RNAmotif (Macke, et al. 2001). A general HHR descriptor
799 (Cervera and De la Peña 2014) was used to detect HHR motifs in *Naiad/Chlamys* and

Hydra elements. More relaxed descriptors were also employed as in Arkhipova, et al. (2017) to accommodate different helices with longer loops and stem mispairing and more relaxed cores with mismatches, and with and without the presence of Helix III, however it did not result in additional HHR motif detection.

Functional characterization of Chlamys elements in Chlamydomonas reinhardtii

The divergence landscape (Fig. S6) and total abundance of *Chlamys* elements in *C. reinhardtii* were calculated using RepeatMasker v4.0.9 (Smit, et al. 2015) and the highly-contiguous assembly of strain CC-1690 (O'Donnell, et al. 2020). The functional characterization represented in Fig. 7 was performed using the standard v5 reference genome. Iso-Seq (accession: PRJNA670202) and H3K4me3 ChIP-seq (accession: PRJNA681680) data were obtained from Gallaher, et al. (2021). CCS (circular consensus sequence) Iso-Seq reads were mapped using minimap2 (-ax splice:hq –secondary no) (Li 2018). Within-species polymorphism was demonstrated by comparison to a *de novo* PacBio-based assembly of the divergent field isolate CC-2931, which exhibits ~3% genetic diversity relative to the standard reference strain (Craig, et al. 2019). The sequencing and assembly of the CC-2931 assembly is described in Supp. note. The CC-2931 assembly was mapped to the v5 reference using minimap2 (-ax asm10).

RT phylogeny and EN protein clustering analysis

Initial amino acid sequence alignments were done with MUSCLE (Edgar 2004), with secondary structure assessed by inclusion of TERT PDB files (3kyl, 3du5) using PROMALS3D (Pei, et al. 2008), and were manually adjusted to ensure the presence of each conserved motif at the proper position. Phylogenetic analysis was done with IQ-TREE v1.6.11 (Trifinopoulos, et al. 2016), with the best-fit model chosen by ModelFinder according to Bayesian information criterion, and with 1000 UFBoot replicates to evaluate branch support.

830 Protein clustering of the GIY-YIG EN domain was performed using CLANS (Frickey and
831 Lupas 2004). GIY-YIG ENs from all superfamilies annotated at NCBI (cd00719) were
832 combined with those from PLEs (canonical C-terminal EN+, N-terminal EN+, *Hydra* and
833 *Terminons*). All ENs were reduced to the core domain spanning from the "GIY" motif to
834 the conserved N aa, unless a Zn-finger linker domain was present upstream of the
835 "GIY", in which case this motif was also included (see Fig. S2). Several very distantly
836 related EN superfamilies were excluded after a preliminary analysis. CLANS was run
837 with a p-value threshold of $1x10^{-8}$ until no further changes were observed in clustering.

838

839 **Acknowledgments**

840

841 This work was supported by the U.S. National Institutes of Health grant R01GM111917
842 to I.A. R.C. was supported by the Biotechnology and Biological Sciences Research
843 Council EASTBIO Doctoral Training Partnership and the project received funding from
844 the European Research Council under the European Union's Horizon 2020 Research
845 and Innovation Programme (Grant Agreement no. 694212).

846

847

848

849

850

851

852

853

854

855

856

857

858 **REFERENCES**

859

860 Arkhipova IR. 2006. Distribution and phylogeny of *Penelope*-like elements in eukaryotes. Syst
861 Biol 55:875-885.
862 Arkhipova IR. 2020. Metagenome proteins and database contamination. mSphere 5:e00854-
863 00820.
864 Arkhipova IR. 2017. Using bioinformatic and phylogenetic approaches to classify transposable
865 elements and understand their complex evolutionary histories. Mob DNA 8:19.
866 Arkhipova IR, Pyatkov KI, Meselson M, Evgen'ev MB. 2003. Retroelements containing introns in
867 diverse invertebrate taxa. Nat Genet 33:123-124.
868 Arkhipova IR, Yushenova IA, Rodriguez F. 2013. Endonuclease-containing *Penelope*
869 retrotransposons in the bdelloid rotifer *Adineta vaga* exhibit unusual structural features and play
870 a role in expansion of host gene families. Mob DNA 4:19.
871 Arkhipova IR, Yushenova IA, Rodriguez F. 2017. Giant reverse transcriptase-encoding
872 transposable elements at telomeres. Mol Biol Evol 34:2245-2257.
873 Baclaocos J, Santesmasses D, Mariotti M, Bierla K, Vetick MB, Lynch S, McAllen R, Mackrill JJ,
874 Loughran G, Guigo R, et al. 2019. Processive recoding and metazoan evolution of
875 selenoprotein P: up to 132 UGAs in molluscs. J Mol Biol 431:4381-4407.
876 Bao W, Kojima KK, Kohany O. 2015. Repbase Update, a database of repetitive elements in
877 eukaryotic genomes. Mob DNA 6:11.
878 Berry MJ, Banu L, Chen YY, Mandel SJ, Kieffer JD, Harney JW, Larsen PR. 1991. Recognition
879 of UGA as a selenocysteine codon in Type I deiodinase requires sequences in the 3'
880 untranslated region. Nature 353:273-276.
881 Böhne A, Zhou Q, Darras A, Schmidt C, Schartl M, Galiana-Arnoux D, Volff JN. 2012.
882 *Zisupton*—a novel superfamily of DNA transposable elements recently active in fish. Mol Biol
883 Evol 29:631-645.
884 Bryszewska MA, Måge A. 2015. Determination of selenium and its compounds in marine
885 organisms. J Trace Elem Med Biol 29:91-98.
886 Camacho C, Coulouris G, Avagyan V, Ma N, Papadopoulos J, Bealer K, Madden TL. 2009.
887 BLAST+: architecture and applications. BMC Bioinformatics 10:421.
888 Castellano S, Novoselov SV, Kryukov GV, Lescure A, Blanco E, Krol A, Gladyshev VN, Guigo
889 R. 2004. Reconsidering the evolution of eukaryotic selenoproteins: a novel nonmammalian
890 family with scattered phylogenetic distribution. EMBO Rep 5:71-77.
891 Cervera A, De la Peña M. 2014. Eukaryotic *Penelope*-like retroelements encode hammerhead
892 ribozyme motifs. Mol Biol Evol 31:2941-2947.
893 Cervera A, de la Peña M. 2020. Small circRNAs with self-cleaving ribozymes are highly
894 expressed in diverse metazoan transcriptomes. Nucleic Acids Res 48:5054-5064.
895 Craig RJ. 2021. The evolutionary genomics of *Chlamydomonas*. University of Edinburgh.
896 Craig RJ, Bondel KB, Arakawa K, Nakada T, Ito T, Bell G, Colegrave N, Keightley PD, Ness
897 RW. 2019. Patterns of population structure and complex haplotype sharing among field isolates
898 of the green alga *Chlamydomonas reinhardtii*. Mol Ecol 28:3977-3993.
899 Craig RJ, Hasan AR, Ness RW, Keightley PD. 2021. Comparative genomics of
900 *Chlamydomonas*. Plant Cell koab026:Online ahead of print.
901 Derbyshire V, Kowalski JC, Dansereau JT, Hauer CR, Belfort M. 1997. Two-domain structure of
902 the td intron-encoded endonuclease I-TevI correlates with the two-domain configuration of the
903 homing site. J Mol Biol 265:494-506.
904 Dunin-Horkawicz S, Feder M, Bujnicki JM. 2006. Phylogenomic analysis of the GIY-YIG
905 nuclease superfamily. Bmc Genomics 7:98.

Dupeyron M, Singh KS, Bass C, Hayward A. 2019. Evolution of Mutator transposable elements across eukaryotic diversity. Mob DNA 10:12.
Edgar RC. 2004. MUSCLE: a multiple sequence alignment method with reduced time and space complexity. BMC Bioinformatics. 5:113.
Eickbush TH. 2002. R2 and related site-specific non-long terminal repeat retrotransposons. Washington, DC: ASM Press.
Eickbush TH, Eickbush DG. 2007. Finely orchestrated movements: evolution of the ribosomal RNA genes. Genetics 175:477-485.
Evgen'ev MB, Arkhipova IR. 2005. *Penelope*-like elements – a new class of retroelements: distribution, function and possible evolutionary significance. Cytogenet Genome Res 110:510-521.
Flutre T, Duprat E, Feuillet C, Quesneville H. 2011. Considering transposable element diversification in *de novo* annotation approaches. PLoS One 6:e16526.
Frickey T, Lupas A. 2004. CLANS: a Java application for visualizing protein families based on pairwise similarity. Bioinformatics 20:3702-3704.
Gabler F, Nam S-Z, Till S, Mirdita M, Steinegger M, Söding J, Lupas AN, Alva V. 2020. Protein sequence analysis using the MPI bioinformatics toolkit. Current Protocols in Bioinformatics 72:e108.
Gallaher SD, Craig RJ, Ganesan I, Purvine SO, McCorkle S, Grimwood J, Strenkert D, Davidi L, Roth MS, Jeffers TL, et al. 2021. Widespread polycistronic gene expression in green algae. Proc Natl Acad Sci U S A 118:e2017714118.
Gladyshev EA, Arkhipova IR. 2009. Rotifer rDNA-specific R9 retrotransposable elements generate an exceptionally long target site duplication upon insertion. Gene 448:145-150.
Gladyshev EA, Arkhipova IR. 2007. Telomere-associated endonuclease-deficient *Penelope*-like retroelements in diverse eukaryotes. Proc Natl Acad Sci U S A 104:9352-9357.
Jiang J, Wang Y, Sušac L, Chan H, Basu R, Zhou ZH, Feigon J. 2018. Structure of telomerase with telomeric DNA. Cell 173:1179-1190.e1113.
Kapitonov VV, Jurka J. 2003. The esterase and PHD domains in CR1-like non-LTR retrotransposons. Mol Biol Evol 20:38-46.
Katoh K, Standley DM. 2013. MAFFT multiple sequence alignment software version 7: improvements in performance and usability. Mol Biol Evol 30:772-780.
Kim KS, Kustu S, Inwood W. 2006. Natural history of transposition in the green alga *Chlamydomonas reinhardtii*: Use of the AMT4 locus as an experimental system. Genetics 173:2005-2019.
Kojima KK, Fujiwara H. 2005. An extraordinary retrotransposon family encoding dual endonucleases. Genome Research 15:1106-1117.
Koyama T, Kondo H, Aoki T, Hirono I. 2013. Identification of two *Penelope*-like elements with different structures and chromosome localization in kuruma shrimp genome. Mar Biotechnol (NY) 15:115-123.
Labunskyy VM, Hatfield DL, Gladyshev VN. 2014. Selenoproteins: molecular pathways and physiological roles. Physiological Reviews 94:739-777.
Letunic I, Bork P. 2019. Interactive Tree Of Life (iTOL) v4: recent updates and new developments. Nucleic Acids Res 47:W256-W259.
Letunic I, Khedkar S, Bork P. 2020. SMART: recent updates, new developments and status in 2020. Nucleic Acids Research 49:D458-D460.
Li H. 2018. Minimap2: pairwise alignment for nucleotide sequences. Bioinformatics 34:3094-3100.
Lin X, Faridi N, Casola C. 2016. An ancient transkingdom horizontal transfer of *Penelope*-like retroelements from arthropods to conifers. Genome Biol Evol 8:1252-1266.
Lingner J, Hughes TR, Shevchenko A, Mann M, Lundblad V, Cech TR. 1997. Reverse transcriptase motifs in the catalytic subunit of telomerase. Science 276:561-567.

957 Low SC, Berry MJ. 1996. Knowing when not to stop: selenocysteine incorporation in
958 eukaryotes. Trends Biochem Sci 21:203-208.
959 Lue NF, Lin YC, Mian IS. 2003. A conserved telomerase motif within the catalytic domain of
960 telomerase reverse transcriptase is specifically required for repeat addition processivity. Mol
961 Cell Biol 23:8440-8449.
962 Macke TJ, Ecker DJ, Gutell RR, Gautheret D, Case DA, Sampath R. 2001. RNAMotif, an RNA
963 secondary structure definition and search algorithm. Nucleic Acids Research 29:4724-4735.
964 Mariotti M, Lobanov AV, Guigo R, Gladyshev VN. 2013. SECISearch3 and Seblastian: new
965 tools for prediction of SECIS elements and selenoproteins. Nucleic Acids Res 41:e149.
966 Mauer K, Hellmann SL, Groth M, Fröbius AC, Zischler H, Hankeln T, Herlyn H. 2020. The
967 genome, transcriptome, and proteome of the fish parasite *Pomphorhynchus laevis*
968 (Acanthocephala). PLoS One 15:e0232973.
969 Neupert J, Gallaher SD, Lu Y, Strenkert D, Segal N, Barahimipour R, Fitz-Gibbon ST, Schroda
970 M, Merchant SS, Bock R. 2020. An epigenetic gene silencing pathway selectively acting on
971 transgenic DNA in the green alga *Chlamydomonas*. Nat Commun 11:6269.
972 Ngan CY, Wong CH, Choi C, Yoshinaga Y, Louie K, Jia J, Chen C, Bowen B, Cheng H, Leonelli
973 L, et al. 2015. Lineage-specific chromatin signatures reveal a regulator of lipid metabolism in
974 microalgae. Nat Plants 1:15107.
975 Nishiyama T, Sakayama H, de Vries J, Buschmann H, Saint-Marcoux D, Ullrich KK, Haas FB,
976 Vanderstraeten L, Becker D, Lang D, et al. 2018. The *Chara* genome: secondary complexity
977 and implications for plant terrestrialization. Cell 174:448-464 e424.
978 Nowell RW, Wilson CG, Almeida P, Schiffer PH, Fontaneto D, Becks L, Rodriguez F, Arkhipova
979 IR, Barraclough TG. 2021. Evolutionary dynamics of transposable elements in bdelloid rotifers.
980 Elife 10:e63194.
981 O'Donnell S, Chaux F, Fischer G. 2020. Highly contiguous Nanopore genome assembly of
982 *Chlamydomonas reinhardtii* CC-1690. Microbiol Resour Announc 9.
983 Pei J, Kim BH, Grishin NV. 2008. PROMALS3D: a tool for multiple protein sequence and
984 structure alignments. Nucleic Acids Res 36:2295-2300.
985 Penton EH, Crease TJ. 2004. Evolution of the transposable element *Pokey* in the ribosomal
986 DNA of species in the subgenus *Daphnia* (Crustacea: Cladocera). Mol Biol Evol 21:1727-1739.
987 Perez-Alegre M, Dubus A, Fernandez E. 2005. REM1, a new type of long terminal repeat
988 retrotransposon in *Chlamydomonas reinhardtii*. Mol Cell Biol 25:10628-10638.
989 Pyatkov KI, Arkhipova IR, Malkova NV, Finnegan DJ, Evgen'ev MB. 2004. Reverse
990 transcriptase and endonuclease activities encoded by *Penelope*-like retroelements. Proc Natl
991 Acad Sci U S A 101:14719-14724.
992 Robinson JT, Thorvaldsdóttir H, Winckler W, Guttman M, Lander ES, Getz G, Mesirov JP. 2011.
993 Integrative Genomics Viewer. Nature Biotechnology 29:24-26.
994 Schön I, Rodriguez F, Dunn M, Martens K, Shribak M, Arkhipova IR. 2021. A survey of
995 transposon landscapes in the putative ancient asexual ostracod *Darwinula stevensoni*. Genes
996 (Basel) 12:401.
997 Schostak N, Pyatkov K, Zelentsova E, Arkhipova I, Shagin D, Shagina I, Mudrik E, Blintsov A,
998 Clark I, Finnegan DJ, et al. 2008. Molecular dissection of *Penelope* transposable element
999 regulatory machinery. Nucleic Acids Res 36:2522-2529.
1000 Smit AFA, Hubley R, Green P. 2015. RepeatMasker Open-4.0. 2013-2015
1001 http://www.repeatmasker.org.
1002 Stoddard BL. 2014. Homing endonucleases from mobile group I introns: discovery to genome
1003 engineering. Mob DNA 5:7.
1004 Storer J, Hubley R, Rosen J, Wheeler TJ, Smit AF. 2021. The Dfam community resource of
1005 transposable element families, sequence models, and genome annotations. Mobile DNA 12:2.
1006 Trifinopoulos J, Nguyen L-T, von Haeseler A, Minh BQ. 2016. W-IQ-TREE: a fast online
1007 phylogenetic tool for maximum likelihood analysis. Nucleic Acids Research 44:W232-W235.

1008 Tujebajeva RM, Copeland PR, Xu XM, Carlson BA, Harney JW, Driscoll DM, Hatfield DL, Berry
1009 MJ. 2000. Decoding apparatus for eukaryotic selenocysteine insertion. EMBO Rep 1:158-163.
1010 Turanov AA, Lobanov AV, Hatfield DL, Gladyshev VN. 2013. UGA codon position-dependent
1011 incorporation of selenocysteine into mammalian selenoproteins. Nucleic Acids Res 41:6952-
1012 6959.
1013 Van Roey P, Meehan L, Kowalski JC, Belfort M, Derbyshire V. 2002. Catalytic domain structure
1014 and hypothesis for function of GIY-YIG intron endonuclease I-TevI. Nat Struct Biol 9:806-811.
1015 Waterhouse AM, Procter JB, Martin DMA, Clamp M, Barton GJ. 2009. Jalview Version 2—a
1016 multiple sequence alignment editor and analysis workbench. Bioinformatics 25:1189-1191.
1017 Wells JN, Feschotte C. 2020. A field guide to eukaryotic transposable elements. Annual Review
1018 of Genetics 54:539-561.
1019 Wen W, Weiss SL, Sunde RA. 1998. UGA codon position affects the efficiency of
1020 selenocysteine incorporation into glutathione peroxidase-1. J Biol Chem 273:28533-28541.
1021 Wicker T, Sabot F, Hua-Van A, Bennetzen JL, Capy P, Chalhoub B, Flavell A, Leroy P,
1022 Morgante M, Panaud O, et al. 2007. A unified classification system for eukaryotic transposable
1023 elements. Nat Rev Genet 8:973-982.
1024 Xu Z, Xin T, Bartels D, Li Y, Gu W, Yao H, Liu S, Yu H, Pu X, Zhou J, et al. 2018. Genome
1025 analysis of the ancient tracheophyte *Selaginella tamariscina* reveals evolutionary features
1026 relevant to the acquisition of desiccation tolerance. Mol Plant 11:983-994.

1027